



Tunable Absorbers Based on an Electrically Controlled Resistive Layer

Changlei Zhang^{1,2} · Cheng Huang¹ · Mingbo Pu¹ · Jiakun Song¹ · Xiangang Luo¹ 

Received: 6 May 2018 / Accepted: 10 July 2018 / Published online: 21 July 2018
© Springer Science+Business Media, LLC, part of Springer Nature 2018

Abstract

In this article, an electrically controlled resistive layer (ECRL) is proposed to construct tunable absorbers. This ECRL is composed of VO₂ film and resistive layer without lithography pattern. The effective resistance of ECRL is numerically verified to be tuned from 18 to 300 Ω/sq as the VO₂ conductivity is changed based on electro-thermally induced insulator-to-metal transition. With such a large tuning range of the effective resistance, the ECRL is utilized to realize a planar tunable bidirectional absorber with absorption efficiency dynamically tuned between 98 and 18% through controlling the conductivity of VO₂. In addition, we demonstrate that the ECRL is also suitable for the design of non-planar tunable absorber. It is still found that the ECRL-based tunable absorbers have the wide angle and polarization-insensitive absorbing properties. These results may be of great interest for tunable absorbing, detecting, smart window, and thermo-solar cell applications.

Keywords Electrically controlled resistive layer · Tunable bidirectional absorber · Tunable broadband absorber · Polarization-insensitive · Terahertz waves

Introduction

In recent years, artificial absorbers that usually used in stealth field, detectors, and thermo-solar cells for their unique feature to absorb electromagnetic wave at a given frequency band such as microwave [1], terahertz [2, 3], infrared [4–6], and visible [7, 8] have attracted significant attention [9, 10]. The absorption characteristics of the conventional artificial absorbers are mainly dependent on the material loss and geometric structures resonance, which are generally unchanged [1–8]. Thus, these absorbers are negligibly influenced by external stimuli such as external fields, temperature, or pressure, offering no chance to tune its electromagnetic response. In order to achieve controllable absorbing characteristics, the active components, such as varactor diode and PIN diode have been reported to construct the tunable absorbers at the microwave region [11, 12]. By tuning the bias voltages applied to the loaded diodes, the absorber can dynamically change its

absorbing characteristics. However, the similar method is not suitable for the higher frequency application, such as terahertz (THz) band and infrared band. To mitigate this issue, the phase change material vanadium dioxide (VO₂), which can be transformed from insulator phase to metal phase at temperature above the insulator-to-metal transition (IMT) temperature (67 °C in bulk crystals) [13], has been recently reported as an active media to achieve tunable absorbers at these frequency bands [14, 15].

The permittivity of VO₂ at room temperature is chosen to be 9 and the conductivity at this situation is about 200 S/m [14]. Furthermore, the conductivity can even reach at 1×10^5 S/m (about 500 times than 200 S/m) when the IMT is realized, usually induced by direct thermal control [16, 17] and photo-thermal effect [18, 19]. However, these control methods are much complex and inconvenient compared with electrically controlled technique. Liu et al. reported an electrically active absorber through Joule heating effect at infrared band [20]. In this article, a mesh-patterned Au layer is adopted to heat the VO₂ thin films, leading to thermally induced IMT. The practicability is limited as the introduction of the mesh-patterned Au layer for the following two main reasons: firstly, the resonance response of the absorber mainly relies on the geometric structure of the Au layer, which limits its application in many fields. Furthermore, the sophisticated techniques, take lithography for instance, are required to fabricate the Au layer, severely increasing the cost of the absorber.

✉ Xiangang Luo
lxg@ioe.ac.cn

¹ State Key Laboratory of Optical Technologies on Nano-Fabrication and Micro-Engineering, Institute of Optics and Electronics, Chinese Academy of Sciences, Chengdu 610209, China

² University of Chinese Academy of Sciences, Beijing 100049, China

In this article, an electrically controlled resistive layer (ECRL) composed of VO₂ and resistive film is proposed to achieve tunable material with predominance of large resistance tuning range and lithography-free feature. Numerical calculation and simulation results show the effective resistance of the active resistive layer can be tuned from 18 Ω/sq (at this situation, the ECRL can act as perfect electrical conductor) to 300 Ω/sq based on the electro-thermally induced insulator-to-metal transition of VO₂. Besides, the ECRL can be achieved directly by the deposition of successive layers with corresponding materials without lithography. With such a large resistance tuning range and lithography-free feature, the ECRL can be flexibly applied in many fields. Here, a tunable bidirectional absorber with the absorption tuned from 98 to 18% around 1 THz and a non-planar tunable absorber with a broad band from 1.08 to 2.5 THz are designed based on the ECRL. The polarization-insensitive feature of the two absorbers is realized due to their symmetrical structures. The designed absorbers are also demonstrated to keep absorption efficiency as high as 80% under incident angle of 60°.

Results

An Electrically Controlled Resistive Layer Based on the IMT of VO₂

The structure of the ECRL which consists of VO₂ layer and resistive layer (a nichrome film with sheet resistance $R_s = 300 \text{ } \Omega/\text{sq}$) is shown in Fig. 1a. As the resistive layer is connected to external bias voltage, Joule heating is produced as a result of the current flow, leading to the electro-thermally induced IMT of VO₂. Thus, the conductivity σ_{VO_2} of VO₂ is changed, indicating that the effective sheet resistances of the VO₂ layer ($R_{\text{VO}_2} = 1 / (\sigma_{\text{VO}_2} \times t_{\text{VO}_2})$) and the ECRL (R_e) can be tuned as a function of the external bias voltage.

Using the transmission line theory, the effective sheet resistance of the ECRL can be expressed by:

$$R_e = \frac{R_{\text{VO}_2} \times R_s}{R_{\text{VO}_2} + R_s} \quad (1)$$

The effective sheet resistance $R_e = 18 \text{ } \Omega/\text{sq}$, $120 \text{ } \Omega/\text{sq}$, and $300 \text{ } \Omega/\text{sq}$ can be obtained when the conductivity σ_{VO_2} values of VO₂ are $1 \times 10^5 \text{ S/m}$, $1 \times 10^4 \text{ S/m}$, and $2 \times 10^2 \text{ S/m}$, respectively. Thus, a large tunable range of R_e is realized by changing the conductivity of VO₂. To support this resistance effective theory, an effective resistance model (ERM) shown in Fig. 1b is investigated. The thickness and permittivity of the ERM are set as $t_{\text{Re}} = t_{\text{VO}_2} + t_{\text{Rs}}$ and 9, respectively. The transmission spectrums of the ECRL and the ERM are respectively shown in Fig. 1a, b. It is seen that the transmission spectrums of the ERM in the case of $R_e = 300 \text{ } \Omega/\text{sq}$, $120 \text{ } \Omega/\text{sq}$, and $18 \text{ } \Omega/\text{sq}$ are almost identical to those of the ECRL as σ_{VO_2} values are $1 \times 10^5 \text{ S/m}$, $1 \times 10^4 \text{ S/m}$, and $2 \times 10^2 \text{ S/m}$, respectively. That means the calculated effective resistance is perfectly matched to the proposed ECRL, and thus a large tuning range of R_e (from 18 to $300 \text{ } \Omega/\text{sq}$) is demonstrated in our design. In addition, there is almost no transmission when the effective sheet resistance $R_e = 18 \text{ } \Omega/\text{sq}$, and so the ECRL can act as a perfect electric conductor (PEC) layer at this situation. The maximal effective sheet resistance only depends on the chosen resistive film, that is to say, a larger tunable range of R_e can be expected for a larger sheet resistance of the resistive film.

A Tunable Bidirectional Absorber

To better explain the potential application of the ECRL, a tunable bidirectional absorber composed of two ECRLs spaced by a 37.5- μm thick quartz is investigated, as shown in Fig. 2. The permittivity of quartz is chosen to be 3.8 supported by [21]. In our design, the two ECRLs displayed in Fig. 2a are the same as the ECRL discussed above. When the normal incident wave illuminates the proposed absorber as situation I, the conductivity of the bottom VO₂ is tuned to be

Fig. 1 **a** Three-dimensional (3D) sketch and the transmission spectrum as a function of σ_{VO_2} for ECRL. **b** 3D sketch and the transmission spectrum as a function of the effective sheet resistance R_e for ERM. $t_{\text{VO}_2} = 500 \text{ nm}$, $t_{\text{Rs}} = 50 \text{ nm}$, and $t_{\text{Re}} = 550 \text{ nm}$

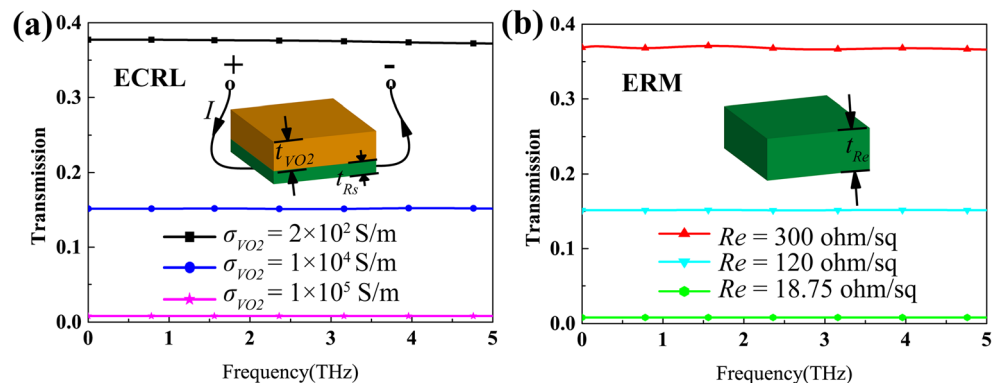
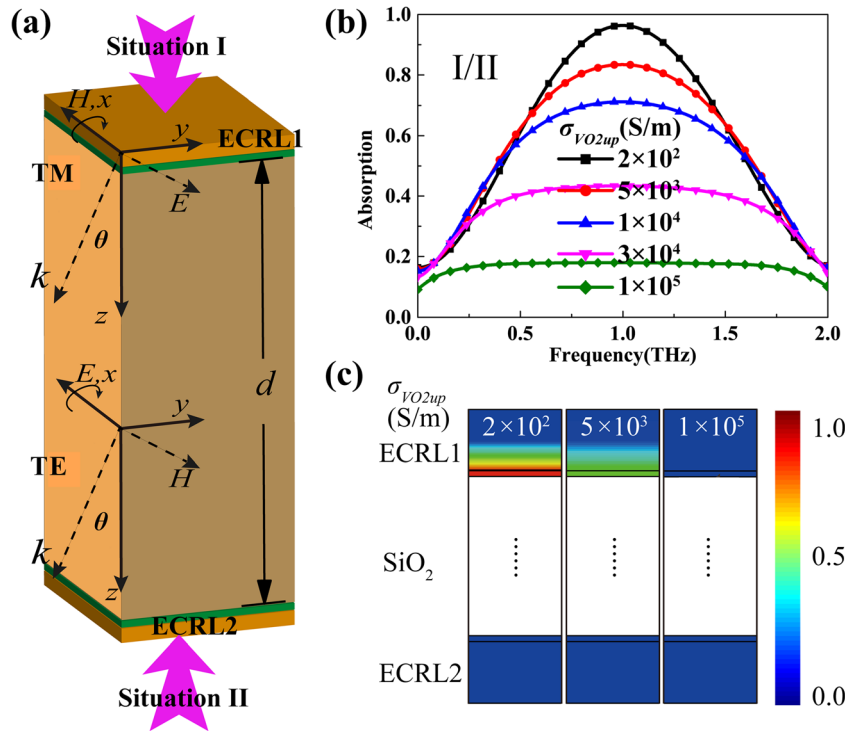


Fig. 2 **a** 3D sketch of the tunable bidirectional absorber. **b** The absorption spectrum of the proposed absorber as a function of σ_{VO2up} under situation I when $\sigma_{VO2down} = 1 \times 10^5$ S/m and situation II when $\sigma_{VO2up} = 1 \times 10^5$ S/m. **c** The power loss density distributions under situation I of the absorber at 1 THz when the conductivity σ_{VO2up} is 200 S/m, 5×10^3 S/m, and 1×10^5 S/m. $d = 37.5 \mu\text{m}$



$\sigma_{VO2down} = 1 \times 10^5$ S/m so that ECRL2 can act as a PEC layer. Then, the absorption of the absorber can be enhanced from 18 to 98% at 1 THz with the conductivity σ_{VO2up} deducing from 1×10^5 to 200 S/m, as seen in Fig. 2b. For the situation II, the ECRL1 is set as a PEC layer by switching the conductivity of top VO₂ to 1×10^5 S/m, and thus, the identical absorption spectrum is obtained when the conductivity of the bottom VO₂ ($\sigma_{VO2down}$) is tuned. Figure 2c shows the power loss density distributions of our absorber at 1 THz when the conductivity σ_{VO2up} is respectively set as 200 S/m, 5×10^3 S/m, and 1×10^5 S/m. It is seen that the strong power loss density is localized around the ECRL1 when the conductivity of σ_{VO2up} is 200 S/m, which means that almost all the incident wave energy is dissipated on the ECRL1. As the σ_{VO2up} is increased to 1×10^5 S/m, the ECRL1 would behave as a PEC layer, reflecting most of the incident wave. Therefore, the power loss density is very weak in our absorber at this case.

The wide-angle absorbing properties of the designed tunable bidirectional absorber are also investigated under oblique incidence at situation I when $\sigma_{VO2up} = 200$ S/m. In the case of TE mode, as shown in Fig. 3a, an obvious absorption band can be observed around 1 THz. High-absorption efficiency about 80% is still kept over the incident angle of 60°. The similar wide-angle absorbing performance of the proposed absorber in TM mode can be also observed in Fig. 3c, and its absorption efficiency is still kept above 80% even at a large oblique incident angle of 80°. In our design, the use of dielectric spacer can decrease the angle sensitivity of the absorber, because the refracted angle in the

high-index material will be reduced according to Snell’s law [22, 23]. Therefore, the wide-angle absorbing property is achieved.

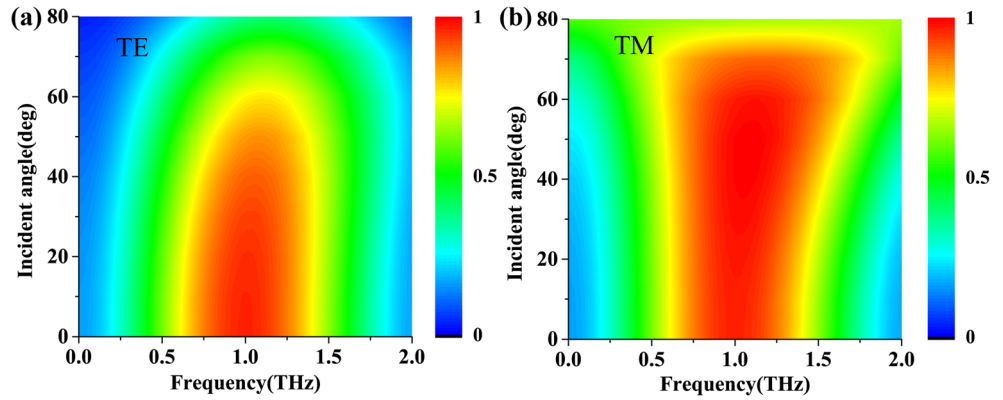
The ECRLs can be regarded as infinitesimally thin resistive sheet for its thickness of 0.55 μm is only about $\lambda/500$ at the frequency of 1 THz. Therefore, the theory of impedance matching is suitable here to explain the absorption mechanism (the situation I when $\sigma_{VO2up} = 200$ S/m and $\sigma_{VO2down} = 1 \times 10^5$ S/m) of the tunable bidirectional absorber. The reflectivity efficiency ($R_1 = 1 - A - T$, see Fig. 2b) of the proposed absorber under normal incidence is about zero when $\sigma_{VO2up} = 200$ S/m and $\sigma_{VO2down} = 1 \times 10^5$ S/m; thus, the boundary conditions for the sheet can be obtained (1 and 2 denote the left side and the right side of the ECRL1, as seen in Fig. 4a) [24, 25]:

$$\begin{aligned} E^1 &= E^2 : I_1 e^{-ik_1 d} + R_1 e^{ik_1 d} = I_2 e^{-ik_2 d} + R_2 e^{ik_2 d} \\ H^1 &= H^2 + J : Y_1 (I_1 e^{-ik_1 d} - R_1 e^{ik_1 d}) = Y_2 (I_2 e^{-ik_2 d} - R_2 e^{ik_2 d}) + J \\ J &= G E^{L(R)} = G (I_2 e^{-ik_2 d} + R_2 e^{ik_2 d}) \end{aligned} \tag{2}$$

where I and R represent the amplitudes of incident and reflective electromagnetic wave. $Y_1 = 1$ and $k_1 = 2\pi/\lambda$ are the admittance and the wavenumber of the free space while $Y_2 = Y_1 \sqrt{\epsilon_r}$ and $k_2 = k_1 \sqrt{\epsilon_r}$ are the admittance and the wavenumber of the dielectric spacer. G is conductance of the ECRL1. Therefore, the reflectivity of the absorber can be expressed as:

$$R_1 = \frac{e^{-ik_1 d}}{2Y_1} [I_2 (Y_1 - Y_2 - G) e^{-ik_2 d} + R_2 (Y_1 + Y_2 - G) e^{ik_2 d}] \tag{3}$$

Fig. 3 Absorption spectrum of the proposed tunable bidirectional absorber as a function of frequency and the incident angle under different polarizations. **a** TE mode and **b** TM mode



In this situation, the reflectivity $R_2 = I_2$ for the ECRL2 is regarded as a PEC layer. The normalized admittance G is nearly equal to Y_1 for the effective resistance of the ECRL1 ($300 \Omega/\text{sq}$) which is matched with free space impedance. Then, the reflectivity R_1 can be further written as:

$$R_1 = R_2 Y_2 e^{-ik_1 d} \frac{e^{ik_1 \sqrt{\epsilon_r} d} - e^{-ik_1 \sqrt{\epsilon_r} d}}{2} = R_2 Y_2 e^{-ik_1 d} \cos\left(\frac{2\pi\sqrt{\epsilon_r} d}{\lambda}\right) \tag{4}$$

The consequence of $\cos\left(\frac{2\pi\sqrt{\epsilon_r} d}{\lambda}\right) = 0$ can be obtained as $R_1 = 0$, which indicates that

$$\sqrt{\epsilon_r} d = \lambda/4 + (n\lambda)/2, n = 0, 1, 2, \dots \tag{5}$$

In our design, the calculated thickness of the absorber is $38.73 \mu\text{m}$ ($n=0$) at 1 THz, which is in a good agreement with the numerical result of $d = 37.5 \mu\text{m}$. To further support this conclusion, the absorption spectrum as a function of the quartz thickness d is investigated as shown in Fig. 4b. There is obvious red shift of the resonance wavelength with the increase of quartz thickness d , which is perfectly matched to the formula above.

A Tunable Broadband Absorber

The ECRL discussed above can also be used to realize non-planar tunable broadband absorber as shown in Fig. 5. The

structure of the absorber indicated in Fig. 5a, b is composed of an ECRL and a gold hemisphere particle spaced by a layer of $16\text{-}\mu\text{m}$ thick quartz and backed by a 200-nm thick gold reflecting layer. In this situation, the sheet resistance of the resistive film in the ECRL is optimized as $R_c = 200 \Omega/\text{sq}$, and the radius of the gold hemisphere particle is $45 \mu\text{m}$. The conductivity of gold is set as $4.561 \times 10^7 \text{ S/m}$ [14]. Our structure can be realized by the deposition of successive layers with corresponding materials on the nanopatterned Al substrate [26]. The order of the deposited materials is VO_2 , nichrome, quartz, and gold. Then, the proposed absorber can be achieved by polishing the deposited gold and corroding the nanopatterned Al substrate. As the structure of the target absorber is symmetrical, the absorption spectrums of the absorber under TE mode and TM mode are the same at normal incidence as illustrated in Fig. 5c. Two obvious absorption peaks can be observed at 1.19 THz and 2.43 THz when the VO_2 is at insulator phase ($\sigma_{\text{VO}_2} = 200 \text{ S/m}$). The corresponding absorption efficiencies reach as high as 99.0 and 99.91% at the above two absorption peaks, respectively. Besides, the absorption efficiency is realized above 90% in a broad band ranging from 1.08 to 2.5 THz, and it can be dynamically controlled by further increasing the conductivity (σ_{VO_2}).

When the VO_2 is at insulator phase, the absorption properties of the designed tunable broadband absorber under oblique incidence are also discussed. As Fig. 6a shows, there is an obvious absorption band from 1.08 to 2.5 THz under TE mode, and the high absorption (70–80%) is still kept at large

Fig. 4 A schematic to explain the absorption mechanism at 1 THz. **a** The sketch map of the electromagnetic wave transmission. **b** The absorption spectrum as a function of the quartz thickness d

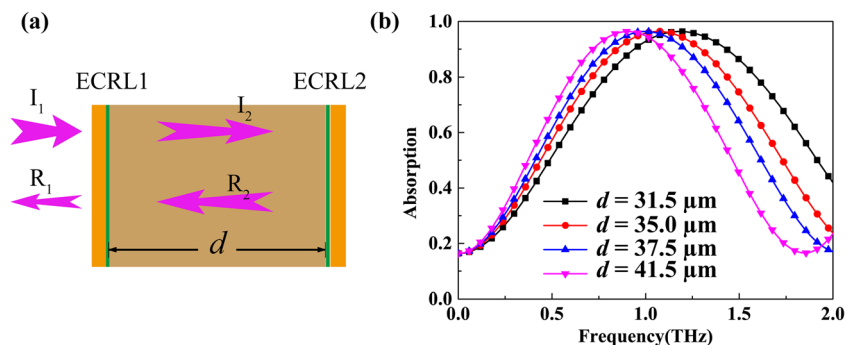
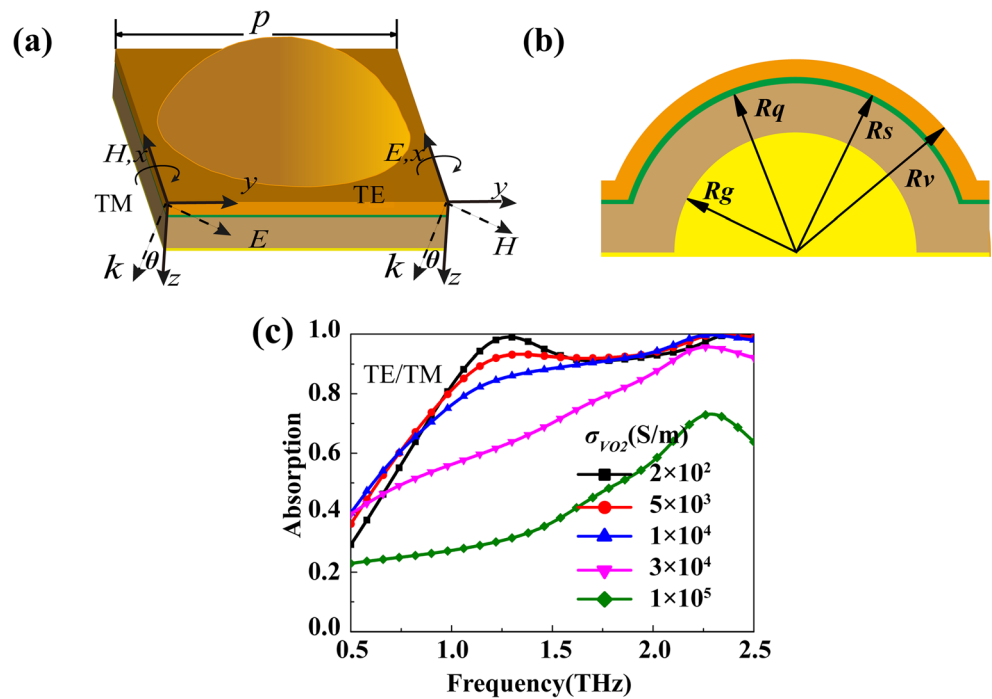


Fig. 5 **a** 3D view and **b** cross-section view of the designed tunable broadband absorber. **c** Absorption spectrum of the target absorber as a function of VO₂ conductivity (σ_{VO_2}) under TE mode and TM mode. $p = 120 \mu\text{m}$, $R_g = 45 \mu\text{m}$, $R_q = 61 \mu\text{m}$, $R_s = 61.05 \mu\text{m}$, $R_v = 61.55 \mu\text{m}$



incidence angle of 60°. For the TM mode, the wide-angle absorbing property is much better, and the absorption efficiency of our absorber is above 90% from 1.05 to 2.5 THz at the oblique incidence of 60°, as seen in Fig. 6b. The angle-insensitive property of the sphere shape in our absorber makes contribution to its wide-angle absorbing capability.

To understand the absorption mechanism at 1.19 THz, the magnetic field and electrical field distributions are studied, as shown in Fig. 7a, b, respectively. The magnetic field is mostly distributed between the neighboring gold hemisphere particles, while the electrical field is enhanced at the area between the units. This phenomenon is caused by the surface plasmon polaritons (SPP) excited at the interface between the gold and dielectric layers due to the additional wave vector originated from the periodic 2D gold hemisphere arrays [27]. Therefore,

the incident wave is strongly localized around the resonator, resulting in the perfect absorption peak at 1.19 THz.

At the other absorption peak, part of the magnetic field energy is localized in the area between the neighboring gold hemisphere particles, as seen in Fig. 7c, which is much analogous to the magnetic field distribution at 1.19 THz, indicating that the SPP also makes contribution to the perfect absorption here. In addition, there is another strong magnetic field localized between the ECRL and the golden hemisphere, resulting in the enhanced electric field around the magnetic distribution as shown in Fig. 7d, which indicates the presence of magnetic resonance (MR) [28]. Thus, due to the combination of the SPP and MR, the incident wave energy is finally dissipated on our absorber.

Fig. 6 Absorption spectrum of the designed tunable broadband absorber as a function of frequency and the incident angle under **a** TE mode and **b** TM mode

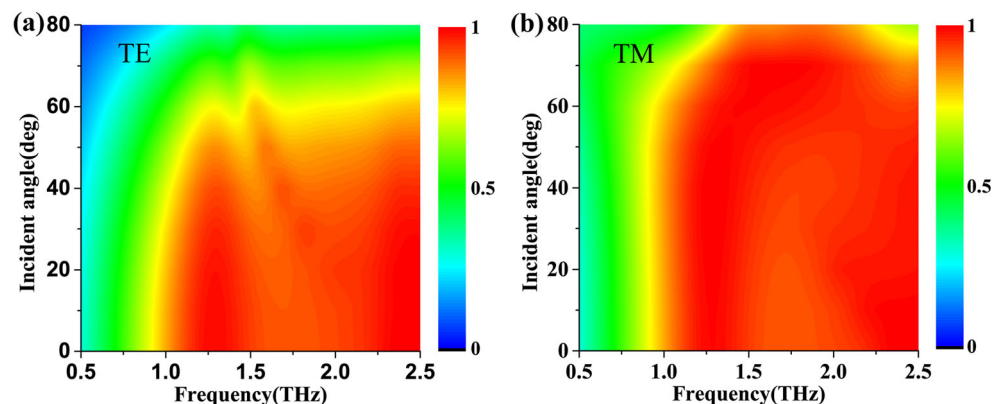
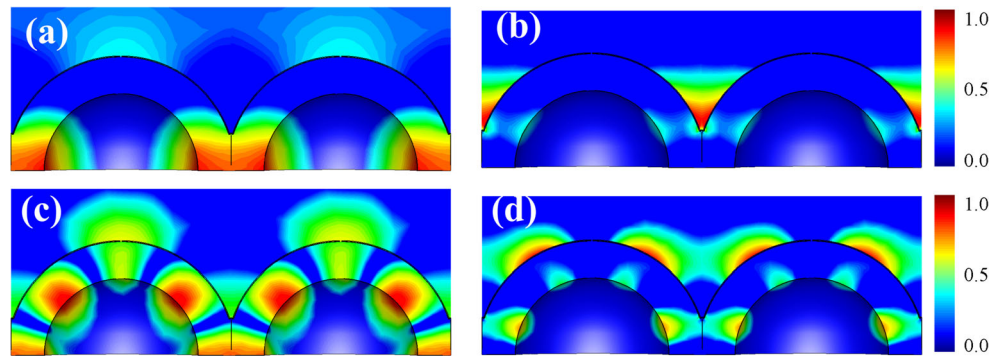


Fig. 7 Sketch map investigating the absorption at 1.19 THz by the distributions of **a** magnetic field and **b** electric field. Side view of **c** magnetic field distribution and **d** electrical field distribution at 2.43 THz



Conclusion

In conclusion, we have proposed and demonstrated a novel electrically controlled resistive layer (ECRL) based on the electro-thermal induced insulator-to-metal transition of VO₂. Thanks to the predominance of large resistance tuning range and lithography-free feature, the ECRL has been utilized to realize a tunable bidirectional absorber and a non-planar tunable broadband absorber here. The polarization-insensitive feature and the wide-angle absorbing property of the above two absorbers support that the ECRL has a wide range applications and profound implications in many fields.

Funding Information This work was sponsored by the National Basic Research (973) Program of China under grant no. 2013CBA01700 and the National Natural Science Foundation of China under grant nos. 61475160, 61605213, and 61775218.

References

- Landy NI, Sajuyigbe S, Mock JJ, Smith DR, Padilla WJ (2008) Perfect metamaterial absorber. *Phys Rev Lett* 100(20):207402
- Chen H (2012) Interference theory of metamaterial perfect absorbers. *Opt Express* 20(7):7165–7172
- Duan G, Schalch J, Zhao X, Zhang J, Averitt RD, Zhang X (2018) Analysis of the thickness dependence of metamaterial absorbers at terahertz frequencies. *Opt Express* 26(3):2242–2251
- Zhang C, Huang C, Pu M, Song J, Zhao Z, Wu X, Luo X (2017) Dual-band wide-angle metamaterial perfect absorber based on the combination of localized surface plasmon resonance and Helmholtz resonance. *Sci Rep* 7(1):5652
- Li J, Yu P, Tang C, Cheng H, Li J, Chen S, Tian J (2017) Bidirectional perfect absorber using free substrate plasmonic metasurfaces. *Adv Opt Mater* 5:1700152
- Chen S, Cheng H, Yang H, Li J, Duan X, Gu C, Tian J (2011) Polarization insensitive and omnidirectional broadband near perfect planar metamaterial absorber in the near infrared regime. *Appl Phys Lett* 99(25):253104
- Han S, Shin JH, Jung PH, Lee H, Lee BJ (2016) Broadband solar thermal absorber based on optical metamaterials for high-temperature applications. *Adv Opt Mater* 4(8):1265–1273
- Qian Q, Sun T, Yan Y, Wang C (2017) Large-area wide-incident-angle metasurface perfect absorber in total visible band based on coupled mie resonances. *Adv Opt Mater* 5(13):1700064
- Luo X (2018) Subwavelength optical engineering with metasurface waves. *Adv Opt Mater* 6(7):1701201
- Luo X (2015) Principles of electromagnetic waves in metasurfaces. *Sci China Phys Mech Astron* 58(9):594201
- Tennant A, Chambers B (2004) A single-layer tunable microwave absorber using an active FSS. *IEEE Microw Wireless Compon Lett* 14(1):46–47
- Mias C, Yap JH (2007) A varactor-tunable high impedance surface with a resistive-lumped-element biasing grid. *IEEE Trans Antennas Propag* 55(7):1955–1962
- Qazilbash MM, Brehm M, Chae BG, Ho PC, Andreev GO, Kim BJ, Kim HT (2007) Mott transition in VO₂ revealed by infrared spectroscopy and nano-imaging. *Science* 318(5857):1750–1753
- Zheng X, Xiao Z, Ling X (2018) A tunable hybrid metamaterial reflective polarization converter based on vanadium oxide film. *Plasmonics* 13(1):287–291
- Yang J, Qu S, Ma H, Wang J, Pang Y (2017) Dual-band tunable infrared metamaterial absorber with VO₂ conformal resonators. *Opt Commun* 402:518–522
- Huang WX, Yin XG, Huang CP, Wang QJ, Miao TF, Zhu YY (2010) Optical switching of a metamaterial by temperature controlling. *Appl Phys Lett* 96(26):261908
- Kats MA, Blanchard R, Genevet P, Yang Z, Qazilbash MM, Basov DN, Capasso F (2013) Thermal tuning of mid-infrared plasmonic antenna arrays using a phase change material. *Opt Lett* 38(3):368–370
- Liu M, Hwang HY, Tao H, Strikwerda AC, Fan K, Keiser GR, Wolf SA (2012) Terahertz-field-induced insulator-to-metal transition in vanadium dioxide metamaterial. *Nature* 487(7407):345–348
- Jeong YG, Han S, Rhie J, Kyoung JS, Choi JW, Park N, Kim DS (2015) A vanadium dioxide metamaterial disengaged from insulator-to-metal transition. *Nano Lett* 15(10):6318–6323
- Liu L, Kang L, Mayer TS, Werner DH (2016) Hybrid metamaterials for electrically triggered multifunctional control. *Nat Commun* 7:13236
- Palik ED (1998) Handbook of optical constants of solids. Academic, San Diego
- Pu M, Ma X, Li X, Guo Y, Luo X (2017) Merging plasmonics and metamaterials by two-dimensional subwavelength structures. *J Mater Chem C* 5(18):4361–4378
- Feng Q, Pu M, Hu C, Luo X (2012) Engineering the dispersion of metamaterial surface for broadband infrared absorption. *Opt Lett* 37(11):2133–2135
- Pu M, Hu C, Wang M, Huang C, Zhao Z, Wang C, Luo X (2011) Design principles for infrared wide-angle perfect absorber based on plasmonic structure. *Opt Express* 19(18):17413–17420
- Knott EF, Shaeffer JF, Tuley MT (2004) Radar cross section. SciTech Publ, Raleigh
- Xiao H, Wang J, Huang H, Lu L, Lin Q, Fan Z, Li D (2015) Performance optimization of flexible a-Si:H solar cells with

- nanotextured plasmonic substrate by tuning the thickness of oxide spacer layer. *Nano Energy* 11:78–87
27. Qu Y, Li Q, Gong H, Du K, Bai S, Zhao D, Qiu M (2016) Spatially and spectrally resolved narrowband optical absorber based on 2D grating nanostructures on metallic films. *Adv Opt Mater* 4(3):480–486
 28. Hu C, Zhao Z, Chen X, Luo X (2009) Realizing near-perfect absorption at visible frequencies. *Opt Express* 17(13):11039–11044